Chemical Science

Accepted Manuscript

This article can be cited before page numbers have been issued, to do this please use: C. Zhang, R. Popov, B. Leforestier, C. Besnard and C. Mazet, *Chem. Sci.*, 2026, DOI: 10.1039/D6SC04784J.

ROYAL SOCIETY OF CHEMISTRY

rsc.li/chemical-science

View Article Online
DOI: 10.1039/D6SC04784J

ARTICLE

Pd-catalyzed regio- and enantioselective allylation of cyclic allylboronates

Received 00th January 20xx,
Accepted 00th January 20xx

DOI: 10.1039/x0xx00000x

Cheng Zhang,[a] Roman Popov,[a] Baptiste Leforestier,[a] Céline Besnard[b] and Clément Mazet*[a]

A robust protocol for the palladium-catalyzed regio- and enantioselective allylic substitution of 6-membered cyclic boronate salts is reported, enabling efficient access to complex scaffolds possessing two distinct alkenes, a synthetic boron handle, and an allylic tertiary stereocenter. This methodology is characterized by high levels of stereoselectivity and regioselectivity across a wide range of substrates. The synthetic potential of this approach has been demonstrated by several transition metal-catalyzed selective derivatizations. Computational studies at a mixed UMA/DFT level of theory reveal that the reaction is governed by a Curtin-Hammett scenario, wherein reductive elimination from hetero-bis-σ-allyl palladium(II) intermediates constitutes the regio- and enantio-determining step of the process.

Introduction

Chiral 1,5-diene segments are not only highly prevalent in natural products (*e.g.* terpenes) and bioactive compounds, but they also frequently serve as versatile building blocks in organic synthesis.[1] The catalytic enantioselective allyl-allyl cross-coupling between prochiral allyl metal reagents and allyl electrophiles offers a direct route to chiral 1,5-dienes.[2-8] In a series of landmark contributions, the Morken group established that allylboronates and allyl carbonates or allyl chlorides could be cross-coupled with excellent levels of regio-, diastereo- and enantioselectivity using Pd catalysis.[2] Chiral 1,5-dienes featuring either one tertiary stereocenter, vicinal tertiary stereocenters or combinations of adjacent tertiary and quaternary stereocenters were accessible by this approach. Subsequently, Feringa and coworkers disclosed a complementary Cu-catalyzed highly regio- and enantioselective cross-coupling between allyl Grignard reagents and linear allyl bromides.[3] Ohmiya and Sawamura showed that Cu catalysis was also effective for the enantioselective cross-coupling of allyl boronates and linear (*Z*)-allyl phosphates. Noticeably, the use of a chiral NHC ligand equipped with a phenoxy group proved indispensable to favor the formation of branched 1,5-dienes over their linear isomers.[4] Carreira reported a chiral iridium–(P,olefin) phosphoramidite complex for the cross-coupling between racemic branched allylic alcohols and allylsilanes to furnish 1,5-dienes with excellent selectivities (Fig. 1-A).[5] More recently, Zhang *et al.* described an asymmetric reductive C(sp^3)–C(sp^3) homocoupling of racemic branched allyl acetates operating through cooperative palladium and photoredox catalysis to afford a broad array of C_2-symmetric 1,5-dienes with vicinal tertiary stereocenters.[6] Even more attractive from a synthetic standpoint are chiral 1,5-dienes which feature additional functional groups that can be further elaborated. Along these lines, the Hoveyda group reported a (NHC)Cu-catalyzed multicomponent protocol combining mono-substituted allenes, a diboron reagent (B_2pin_2) and primary allyl phosphates. In this system, the allyl-copper generated by borylcupration of the allene reacts via a S_N2' mechanism with the allyl electrophile. The resulting enantioenriched 1,5-dienes display a tertiary stereocenter and a trisubstituted (*Z*)-configured alkenylboron unit (Fig. 1-B).[7] A remarkable switch in selectivity was achieved through synergistic Cu/Pd catalysis by Maseras, Fañanás-Mastral and colleagues in a related borylative allyl-allyl cross-coupling (Fig. 1-C).[8] In this process, two adjacent tertiary stereocenters and a vinylborane are installed in one operation with excellent stereoselectivity by means of a single chiral bisphosphine ligand. The success of this approach stems from an inner-sphere S_E2' transmetallation from a Cu-allyl intermediate to a Pd-allyl intermediate.

We recently reported a Cu-catalyzed borylation of unactivated vinylcyclopropanes to form non-symmetrical 6-membered cyclic boronate salts (**1**) and explored their reactivity toward a number of electrophilic reagents.[9] In a subsequent study, we developed Pd-catalyzed regiodivergent C1- and C3-arylations that afford synthetically modular alkenyl boronates. Computational studies served to establish that C3-arylation is governed mostly by steric factors during binding of the substrate to the metal center, whereas a Curtin-Hammett

[a] Department of Organic Chemistry, University of Geneva, 30 quai Ernest Ansermet, 1211 Geneva, Switzerland.
[b] Laboratory of Crystallography, University of Geneva, 24 quai Ernest Ansermet, 1211 Geneva, Switzerland.

View Article Online
DOI: 10.1039/D6SC04784J

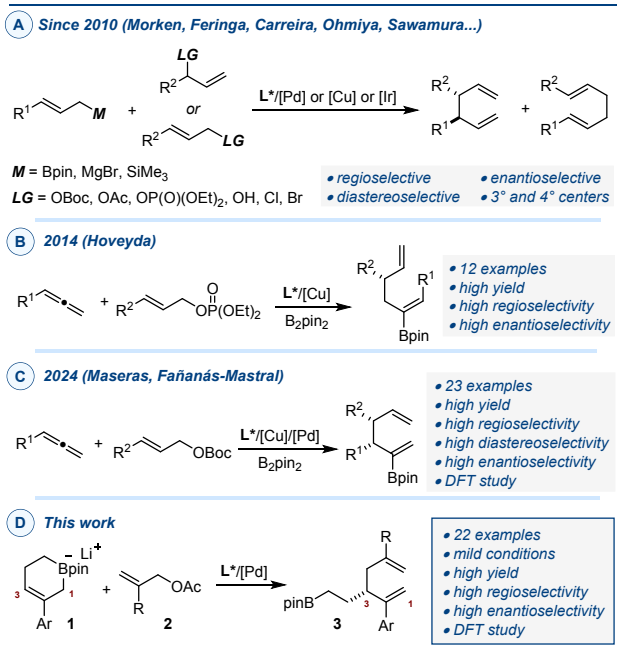

Fig. 1 (A) Pd-, Cu- and Ir-catalyzed regio-, diastereo- and enantioselective allyl-allyl cross-coupling reactions. (B) Cu-catalyzed borylative allylation of allenes. (C) Synergistic [Pd/Cu]-catalyzed borylative allylation of allenes. (D) Pd-catalyzed allylation of 6-membered allylboronates.

equilibrium between two η^2-alkene-Pd intermediates determines C1 selectivity. Even though the level of enantioselectivity remained modest, we further demonstrated that the C3-selective arylation was amenable to asymmetric catalysis.[10] Prior to our work, the Fujihara group had described the preparation of isolable, well-defined, 5-membered cyclic allylboronates by Cu catalysis starting from 1,3-dienes and B_2pin_2.[11] Of note, in a recent communication, they reported the (non-catalytic) allylation of these compounds using allyl bromides to produce a small collection of racemic boron-containing 1,5-dienes.[12]

In this manuscript, we report a protocol for the Pd-catalyzed regio- and enantioselective allylic substitution of 6-membered cyclic boronate salts (**1**) at C3 to deliver products featuring two distinct alkenes, an allylic tertiary stereocenter and a synthetically modular boron handle (**3**) (Fig. 1-D). The process provides high levels of regio- and enantioselectivity across a broad range of substrates combinations. The synthetic utility of the products is highlighted through a series of transition metal-catalyzed selective derivatizations. Mechanistic investigations based on a computational study point to a system under Curtin-Hammett control where discrimination between competing reductive eliminations from hetero-bis-s-allyl palladium(II) intermediates is responsible for the high levels of regio- and enantioselectivity obtained.

Results and discussion

Table 1. Reaction optimization.[a]

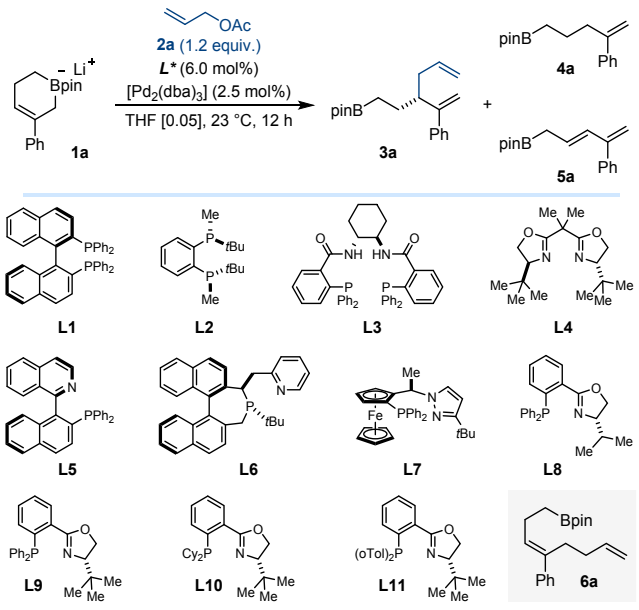

entry	L*	3a (%)[b]	4a (%)[b]	5a (%)[b]	er_{3a}[c]
1	**L1**	93	-	-	53 : 47
2	**L2**	18	38	-	82 : 18
3	**L3**	<5	-	38	*nd*
4	**L4**	-	-	-	*nd*
5	**L5**	47	-	-	77 : 23
6	**L6**	54	-	-	82.5 : 17.5
7	**L7**	42	-	-	60 : 40
8	**L8**	86	-	-	87.5 : 12.5
9	**L9**	75	-	-	92.5 : 7.5
10	**L10**	19	-	-	75.5 : 24.5
11	**L11**	85	-	-	94 : 6
12[d]	**L11**	80	-	-	95 : 5
13[e]	**L11**	70	-	-	96 : 4

[a] Reaction conditions: 1a (0.1 mmol). [b] Determined by ^{1}H NMR analysis of the crude reaction mixture using an internal standard. [c] Determined by HPLC using a chiral stationary phase after oxidation to the corresponding alcohol. [d] At 0 °C for 12 h. [e] At –20 °C for 48 h.

Reaction development. Preliminary investigations consisted in evaluating a representative selection of chiral ligands using cyclic boronate salt **1a** and allyl acetate **2a** as model substrates (Table 1). While Binap (**L1**) delivered the targeted product quantitatively but in nearly racemic form, BenzP* (**L2**) gave **3a** in much reduced NMR yield but with a promising level of enantioinduction (entries 1–2). The latter experiment showed substantial formation of alkenylboronate **4a**, which results from a formal protonation of **1a**. No reaction was observed with **L3**, an archetypical chiral ligand successfully employed in countless

View Article Online
DOI: 10.1039/D6SC04784J

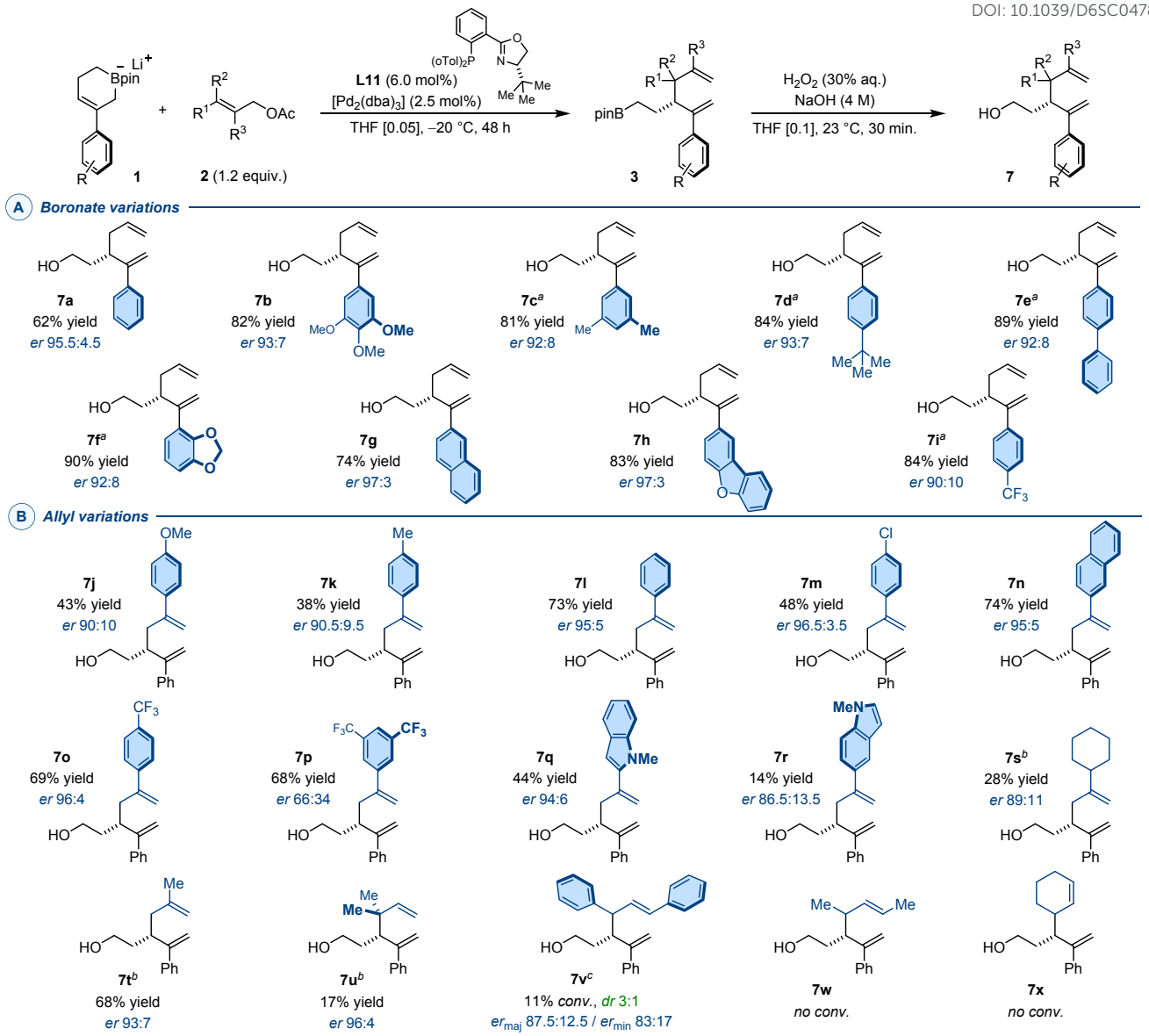

Fig. 2 Scope of the Pd-catalyzed C3-selective allylation of cyclic allylboronates (0.3 mmol scale). Regioselectivity >25:1 in all cases as determined by ^{1}H NMR spectroscopy after allylation using an internal standard. Yield over two steps after oxidation to the corresponding alcohol and purification by column chromatography. [a] THF/DMF (20:1), 23 °C, 24 h. [b] At 23 °C. [c] The relative stereochemistry for **7v** could not be determined unambiguously.

asymmetric allylic alkylation reactions (entry 3).[13] In contrast, dienylboronate **5a** was the only detectable product with bisoxazoline **L4** (entry 4). This side-product was also detected using Quinap (**L5**) together with the desired allylation product **3a** (77:23 er_{3a}; entry 5). The most promising results were subsequently obtained with other (P,N) ligands (**L6–L11**), with derivatives of the phosphinooxazoline family offering the best balance between reactivity and selectivity (entries 6–11). With the best performer (**L11**), the level of enantioinduction could be further improved by reducing the temperature and extending the reaction time (entries 12–13). Thus, performing the allylation reaction at –20 °C for 48 h afforded **3a** in 70% NMR yield and 96:4 *er*. Of important note, compound **6a** that would result formally from a C1-selective allylation reaction was never observed during this optimization campaign.[10] Finally, other allyl electrophiles did not provide improved performances and focus was therefore placed on the use of readily available allyl acetates (See SI).

The generality of the Pd-catalyzed allylation reaction was explored using these optimal reaction conditions. As observed with the model reaction, C3/C1 regioselectivity was systematically >25:1. Variations of the structure of the cyclic boronate salts (**1**) were first carried out (Fig. 2-A). For derivatives that were only sparingly soluble in THF, we ran the reaction in a 20:1 THF/DMF solvent mixture at 23 °C for 24 h. For the sake of practicality, all products were isolated after nearly quantitative alkali oxidation to the corresponding alcohols (**7**). We observed that substrates with an electron-

View Article Online
DOI: 10.1039/D6SC04784J

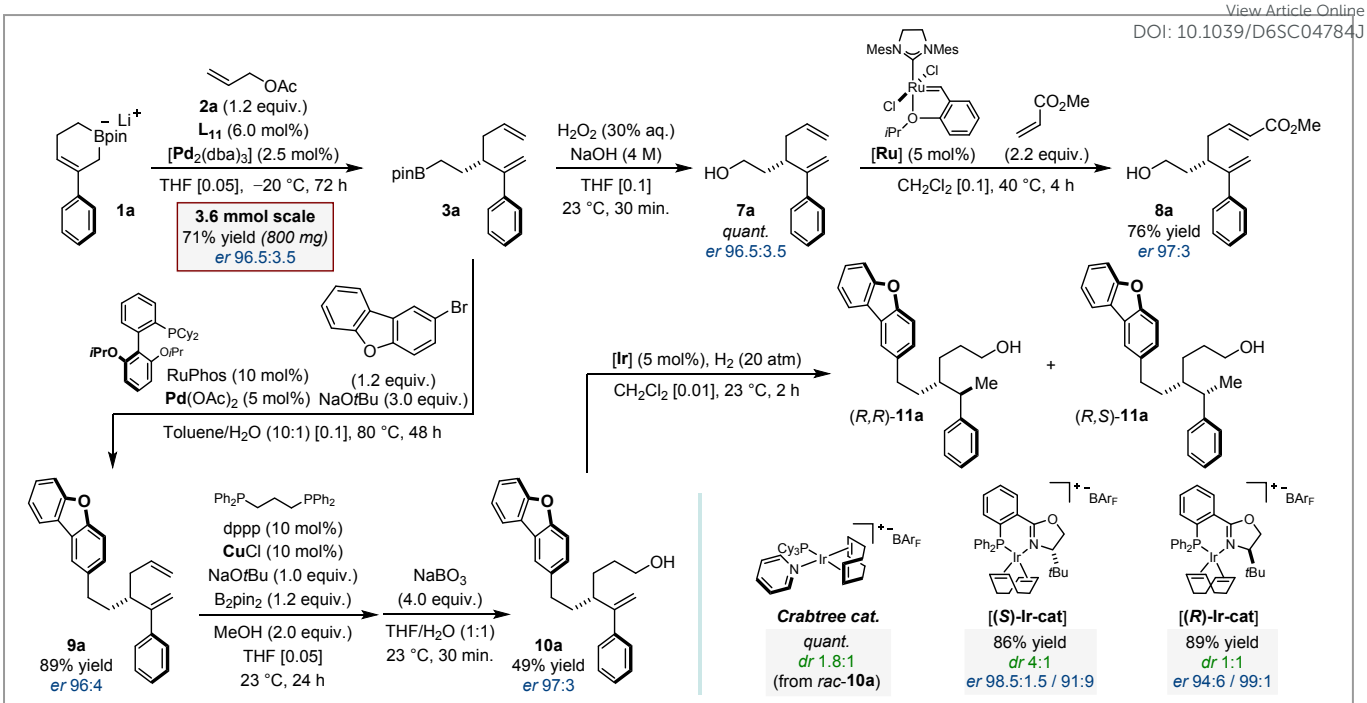

Fig. 3 Gram-scale experiment for the Pd-catalyzed C3-selective allylation of cyclic allylboronates **1a** (3.6 mmol scale) and selective transition metal-catalyzed derivatizations of **3a** (0.05–0.30 mmol scale).

neutral or an electron-rich aryl group underwent catalysis efficiently, delivering the products in high yield and excellent levels of enantiocontrol (**7a–7h**). A slight decrease in enantioselectivity was observed when a *p*-trifluoromethyl group was introduced (**7i**: 90:10 *er*). Structural variations of the allyl acetate precursor (**2**) led us to identify 2-substituted derivatives as the most suitable candidates with the optimized reaction conditions (Fig. 2-B). Whereas electron-rich electrophilic substrates led to moderate yield and slightly reduced enantiomeric ratio (**7j-k**), electron-neutral and electron-deficient precursors afforded the allylation product in systematically high yield and in enantiomeric ratio ≥95:5 (**7l–7o**). The level of enantioinduction dropped markedly when two trifluoromethyl substituents were introduced in *meta* positions of the aryl substituent (**7p**). Connecting an *N*-methyl indole by the 2-position to the allyl unit led to appreciable performances (**7q**), while an isomeric structure connected by the 5-position showed poor reactivity and lower level of enantioinduction (**7r**). 2-Alkyl substituted allyl acetates were also found to be competent substrates with the optimized reaction conditions. While 2-methylallyl acetate generated **7t** in 68% yield and 93:7 *er*, 2-cyclohexylallyl acetate afforded **7s** in 89:11 *er* but in only 28% yield, presumably due to more pronounced steric hindrance. Even though the yield of the product was very low, using isoprenyl acetate, we established that the catalytic method enables the installation of a quaternary center adjacent to the tertiary stereocenter whilst maintaining a high level of enantiocontrol (**7u**: 96:4 *er*). Allyl derivatives with identical substituents at C1 and C3 are a important substrate subclass for enantioselective allylic substitutions.[13d] Using racemic 1,3-diphenylprop-2-enyl acetate, the catalytic activity was rather low and **7v** was generated as a 3:1 diastereomeric mixture, each isomer being obtained with relatively similar levels of enantiocontrol (**7v**: 87.5:12.5 er_{maj} / 83:17 er_{min}). No reaction was observed starting from racemic 1,3-dimethylprop-2-enyl acetate or from racemic cyclohexyl acetate. The absolute configuration of the allylation products was established by analogy after X-ray analysis of a derivative of **7e** (See SI).

The robustness of the protocol was established by conducting the Pd-catalyzed enantioselective allylation of cyclic allylboronates on a 3.6 mmol scale using **1a** and allyl acetate **2a** to afford the product (**3a**) as a yellow oil without any erosion of the reactivity or the enantioselectivity (71% yield, 96.5:3.5 er_{3a}) (Fig. 3). Next, we sought to demonstrate the synthetic utility of the product of catalysis through a series of selective transition metal-catalyzed derivatizations. After quantitative alkali oxidation of **3a** to **7a**, we showed that methyl acrylate reacts preferentially with the terminal alkene when engaged in a subsequent Ru-catalyzed cross-metathesis using Hoveyda-Grubbs precatalyst to generate **8a** (76% yield, 97:3 er_{8a}). In parallel, **9a** was obtained in 89% yield (96:4 er_{9a}) when **3a** was engaged in a Pd-catalyzed cross-coupling reaction using 2-bromodibenzofuran as electrophile.[14] Subsequently, a highly chemo- and regioselective Cu-catalyzed protoboration of the terminal alkene furnished **10a** after oxidation of the resulting boronate to the corresponding primary alcohol (49% over two steps, 97:3 er_{10a}). The diastereoselective hydrogenation of 1,1-disubstituted alkenes is challenging, in particular for substrates with a potentially labile stereocenter in allylic position such as **10a**.[15] Using Pfaltz's modified version of the Crabtree catalyst, **11a** was generated quantitatively. The 1.8:1 diastereomeric mixture obtained provides a measure of the bias imposed by the stereocenter present in the substrate. With the (*S*) enantiomer of a commonly employed iridium-based

View Article Online
DOI: 10.1039/D6SC04784J

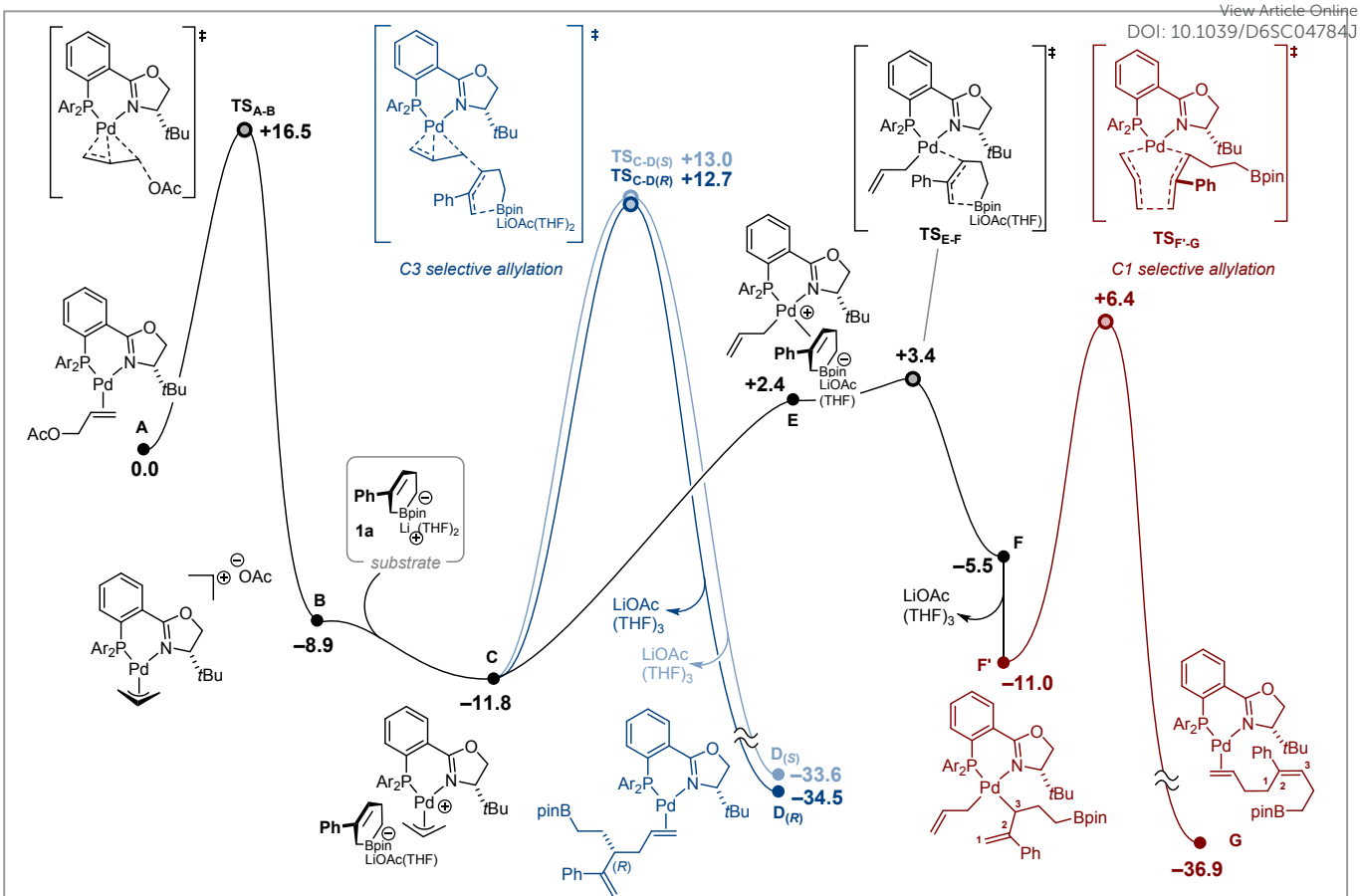

Fig. 4 Computed free energy reaction profile (kcal/mol, 253.15 K) for the Pd-catalyzed C3-selective allylation of cyclic allylboronate **1a** via an outer sphere mechanism (blue) and alternative pathway via a hetero-bis-σ-allyl intermediate. Level of theory: (ωB97M-V/def2-TZVPD//UMA-s-1p1)ALPB(THF), ORCA 6.1.0.[17]

hydrogenation precatalyst ([**(*S*)-Ir-cat**]),[16] the diastereomeric ratio increased to 4:1 (*match case*), while with the catalyst of opposite absolute configuration, the *dr* was only 1:1 (*mismatch*). The variations of the enantiomeric ratio with respect to **10a** measured in both cases point to a complex mechanistic scenario in which concurrent isomerization transiently generating the (*E*) and (*Z*) stereoisomers of a tetrasubstituted alkene is likely to occur.[18]

Computational study. Mechanistic investigations were performed computationally. Building on the methodology established in our previous study on the Pd-catalyzed arylation of the cyclic boronate salts,[10] the speciation of **1a** in THF with respect to aggregation and microsolvation was examined by molecular dynamics simulations. Thus, **1a** was placed in a spherical cell containing 25 THF molecules bounded by repulsive harmonic walls, with the sphere radius adjusted to match the experimental density of THF (see SI, section 8.1), and left to equilibrate over the course of 50 ps at 300 K. The lowest free energy configuration for **1a** was determined to feature two explicit molecules of THF coordinated to the lithium atom, the latter being chelated by the substrate via one oxygen atom of the (pinacolato)boron unit and the alkene. A dimeric form of **1a** featuring bridging lithium cations was similarly placed in a spherical cell containing 29 THF molecules and left to equilibrate for 50 ps. Spontaneous dissociation into two microsolvated monomers was observed rapidly, further suggesting the monomeric nature of **1a** in THF. Anticipating the potential dissociation of LiOAc over the course of the reaction, the microsolvation of LiOAc was also investigated and led to the identification of LiOAc(THF)$_3$ as the most favorable species.[19]

While the use of UMA for full studies on catalytic cycles is only emerging in the literature,[10,20] our benchmark calculations on selected geometries showed excellent agreement with the reference DFT level of theory as well as DLPNO-CCSD(T) (see SI). Our initial mechanistic hypothesis was inspired by a scenario recently proposed by Kan, Li and Wu, whereby an oxidative addition leads to a cationic Pd-allyl intermediate that subsequently undergoes a direct outer-sphere nucleophilic attack by the alkene of the boronate salt.[21] The corresponding computed profile is displayed in Fig. 4 (**A→D**) and begins with oxidative addition of allyl acetate to the phosphinooxazoline palladium(0) complex **A** (**TS$_{A-B}$**; $\Delta G^{\ddagger}$ = 16.5 kcal/mol) to deliver the corresponding cationic π-allyl Pd(II) intermediate **B** at –8.9 kcal/mol. The magnitude of the corresponding activation energy is consistent with that calculated for similar systems by Bellido *et. al.*.[22] Subsequent association of the substrate **1a** is slightly favored, with the catalyst–substrate adduct **C** located at –11.8 kcal/mol. From **C**, an outer-sphere nucleophilic addition

View Article Online
DOI: 10.1039/D6SC04784J

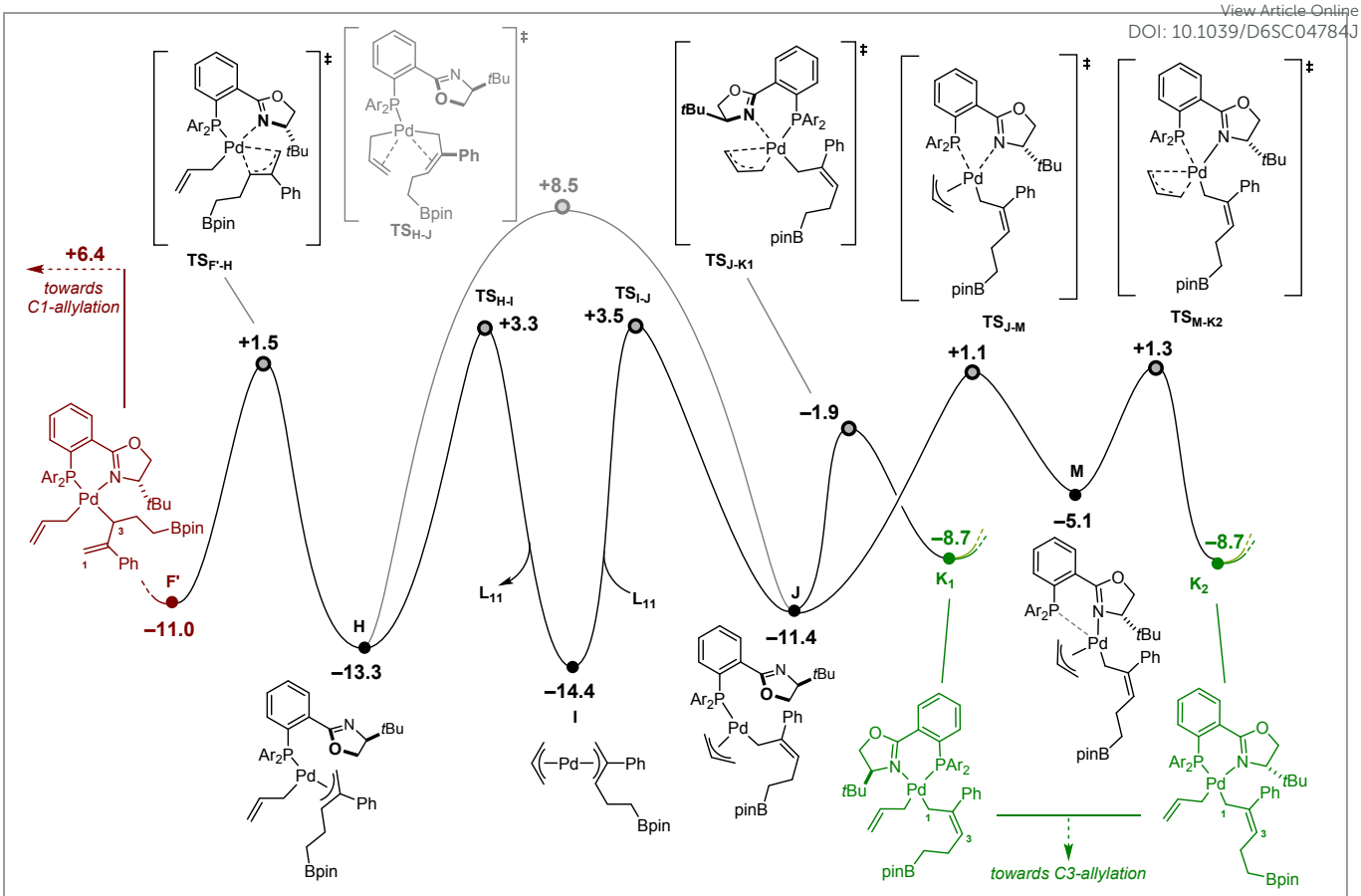

Fig. 5 Computed free energy reaction profile (kcal/mol, 253.15 K) for the reversible isomerization of pro-C1 hetero-bis-σ-allyl complex **F'** into pro-C3 hetero-bis-σ-allyl complexes **K$_1$** and **K$_2$**. Level of theory: (ωB97M-V/def2-TZVPD//UMA-s-1p1)ALPB(THF), ORCA 6.1.0.[17]

of the C=C bond of the boronate to the electrophilic π-allyl-Pd complex irreversibly provides the very exergonic product-bound Pd(0) intermediates **D$_{(R)}$** and **D$_{(S)}$**. The corresponding diastereomeric transition states were calculated at **TS$_{C\text{-}D(R)}$** at +12.7 and **TS$_{C\text{-}D(S)}$** at +13.0 kcal/mol respectively ($\Delta\Delta G^{\ddagger}$ = 0.3 kcal/mol) (Fig. 4, blue pathways).[23] Although these results are in line with the stereochemical and regiochemical outcomes of the reaction observed experimentally, the corresponding overall barriers from **C** (24.5–24.8 kcal/mol) are not consistent with a reaction occurring at –20 °C and underline the need to identify a kinetically more accessible manifold. We first assumed that dissociation of the LiOAc salt from the substrate would enhance the nucleophilicity of the cyclic allylboronate, but this approach only yielded transition states higher in energy (see SI, section 8.3.3).

In our previous study on the Pd-catalyzed C3-selective arylation of cyclic boronate salts,[10] two distinct activation modes were identified, proceeding via (i) direct ring-opening electrophilic substitution at the Pd center or (ii) coordination of the alkene and followed by ring-opening. While electrophilic substitution did not yield a more favorable pathway (see SI, section 8.3.3), η^2-coordination of **1a** *trans* to the P atom of the ancillary ligand accompanied by concomitant π→σ isomerization of the allyl fragment is accessible, albeit uphill (intermediate **E**, +2.4 kcal/mol). The ensuing ring-opening is near barrierless, with **TS$_{E\text{-}F}$** located at only +3.4 kcal/mol, affording the bis-σ-allyl Pd(II) complex **F** at –5.5 kcal/mol. Further stabilization by dissociation of LiOAc away from the overall neutral Pd(II) fragment generates **F'** at –11.0 kcal/mol. Similar bis-σ-allyl Pd(II) complexes have been described in the literature by Echavarren,[24] Álvarez and Espinet,[25] Morken,[2a,2e] and more recently by Maseras and Fañanás-Mastral.[8] In particular, they have been shown to favor 3-3' reductive elimination over the canonical 1-1' pathway. This preferred reactivity pattern was verified with our system, with the reductive elimination transition state **TS$_{F'\text{-}G}$** located at +6.4 kcal/mol being the most accessible to afford **G** irreversibly (see SI, section 8.3.6). While this pathway is favored by more than 6 kcal/mol over the outer sphere mechanism described above (**A→D**), it unfortunately diverts the system towards the formation of a C1-allylation regioisomer that was never observed experimentally (Fig. 4, crimson-red pathway).

At this stage, we reasoned that an isomeric structure of **F'** where the two allyl fragments would be well-poised for a subsequent C3-selective reductive elimination might be accessible through successive σ/π-allyl isomerizations of both allyl units. Such a pathway could be identified and is displayed in Fig. 5. We found that σ-to-π isomerization of the substrate-derived allyl fragment was accompanied by decoordination of the *N*-donor of the oxazoline ring to access the slightly more stable intermediate **H** at –13.3 kcal/mol via a modest barrier (**TS$_{F'-H}$** at +1.5 kcal/mol). From **H**, a direct intramolecular σ/π

View Article Online
DOI: 10.1039/D6SC04784J

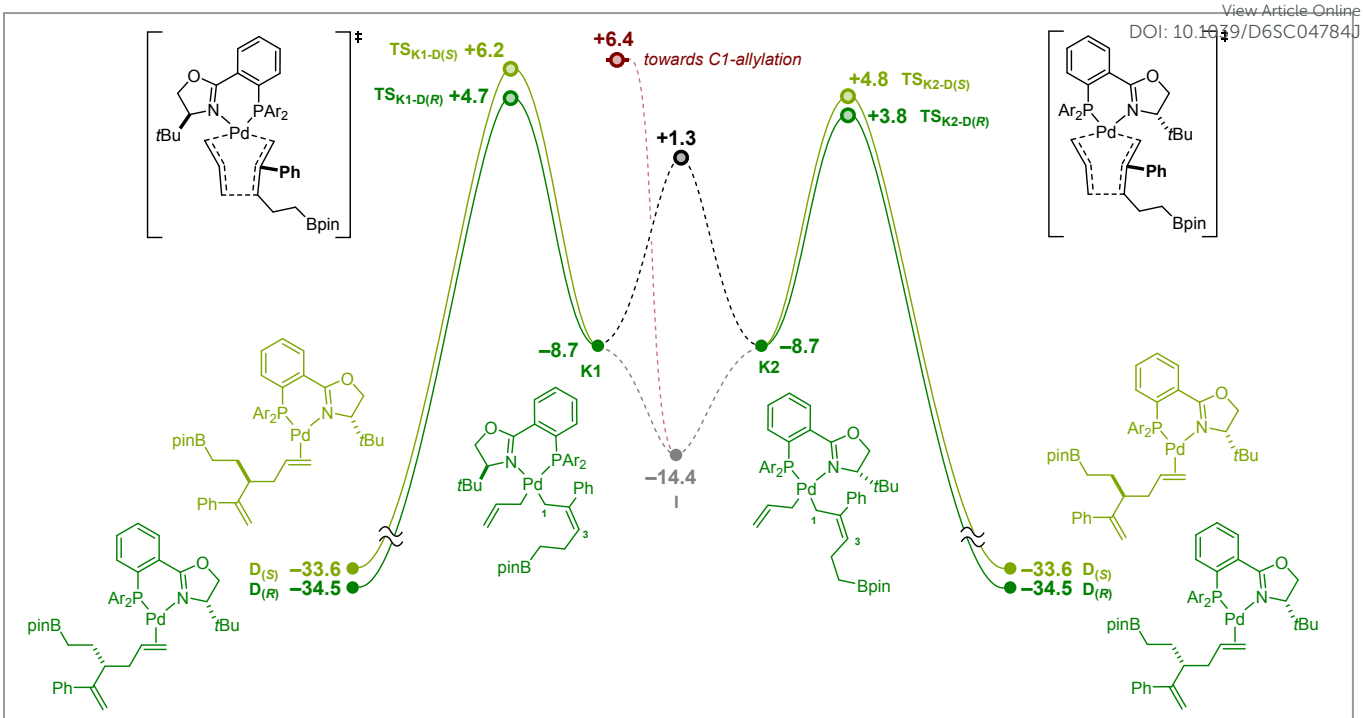

Fig. 6 Summarized free energy profile (kcal/mol, 253.15 K) for the Curtin-Hammett control between $\mathbf{K_1}$ and $\mathbf{K_2}$ and corresponding pro-(*R*) and pro-(*S*) reductive elimination transition states affording Pd-bound C3-allylation products $\mathbf{D_{(R)}}$ and $\mathbf{D_{(S)}}$, respectively. Level of theory: (ωB97M-V/def2-TZVPD//UMA-s-1p1)ALPB(THF), ORCA 6.1.0.[17]

exchange in which the substrate-derived allyl returns to σ-bonding (retaining C1–Pd connectivity) concomitant with σ–π conversion of the second allyl to give **J** was found to occur via $\mathbf{TS_{H–J}}$ at +8.5 kcal/mol (grey pathway). Although mechanistically reasonable, this barrier is kinetically disfavored relative to the competing **F′→G** pathway leading to the C1-regioisomer ($\mathbf{TS_{F′-G}}$ at +6.4 kcal/mol) (Fig. 5). Instead, perhaps counterintuitively, the lowest accessible manifold we could identify from **H** proceeds by σ-to-π isomerization of the second allyl fragment, which is coupled with decoordination of ligand **L11** to furnish the hetero-bis(η³-allyl) palladium(II) intermediate **I** (ΔG = −14.4 kcal/mol) via $\mathbf{TS_{H-I}}$ at only +3.3 kcal/mol. Coordination of the P atom of **L11** from the opposite side enables formation of a σ-C1-allyl complex while maintaining π-coordination of the simple allyl unit, to afford **J** located at −11.4 kcal/mol via $\mathbf{TS_{I-J}}$ at +3.5. Subsequent chelation by both donor atoms of the phosphinooxazoline ligand gives $\mathbf{K_1}$ (at −8.7 kcal/mol) through $\mathbf{TS_{J–K1}}$ (−1.9 kcal/mol). Equilibration of $\mathbf{K_1}$ to $\mathbf{K_2}$ (also at −8.7 kcal/mol) occurs readily via a shallow interconversion surface that passes through intermediate **M** at −5.1 kcal/mol and low-lying transition structures at +1.1 and +1.3 kcal/mol. Importantly, the isomeric structures of $\mathbf{K_1}$ and $\mathbf{K_2}$ both place the allyl termini in the arrangement required to access the C3-allylation product via a reductive elimination involving the remote carbon atoms of the σ-allyl fragments. Collectively, the above-described isomerization events enable complete interconversion between **F′**, $\mathbf{K_1}$, and $\mathbf{K_2}$, placing the system under Curtin–Hammett control. As a corollary, neither regio- nor enantioselectivity are determined by the relative populations of these intermediates, but rather by the free-energy differences between the competing reductive-elimination transition states accessible from each path. This relationship is summarized in Fig. 6, which shows that the C3-selective reductive eliminations originating from $\mathbf{K_1}$ and $\mathbf{K_2}$ are uniformly lower in energy than the C1-selective pathway from **F′**. Moreover, in agreement with experimental observations, for both $\mathbf{K_1}$ and $\mathbf{K_2}$, the pro-(*R*) transition state is consistently favored over the corresponding pro-(*S*) transition state. From $\mathbf{D_{(R)}}$, release of the product and coordination of another equivalent of allyl acetate was calculated to be downhill by 4.8 kcal/mol (See SI, Section 8.3.7). Therefore, the overall catalytic cycle is predicted to proceed with an apparent free-energy barrier of 18.2 kcal/mol, defined by the energy span between **I** and $\mathbf{TS_{K2–D(R)}}$, a magnitude fully compatible with the optimized reaction conditions.[26,27] Of note, within the intrinsic uncertainty of DFT, this turnover-limiting event may be kinetically competitive with the initial oxidative addition of allyl acetate.

Conclusions

In conclusion, we have developed a protocol for the palladium-catalyzed regio- and enantioselective allylic substitution of 6-membered cyclic boronate salts. This catalytic reaction provides efficient access to valuable scaffolds possessing two distinct alkenes, a synthetic boron handle, and an allylic tertiary stereocenter. This methodology features high levels of regio- and enantioselectivity across an array of structurally diversified substrates, and its synthetic utility was illustrated through various transition metal-catalyzed derivatizations. Computational studies at a mixed UMA/DFT level of theory

indicate that the reaction is governed by a Curtin-Hammett scenario, where high stereo- and regioselectivity are achieved through controlled reductive elimination from hetero-bis-σ-allyl palladium(II) intermediates.

Author contributions

The manuscript was written through the contributions of all authors, and all authors have given approval to the final version.

Conflicts of interest

There are no conflicts to declare.

Data availability

The data supporting this article have been included as part of the SI. This includes experimental procedures, characterization of all new compounds, spectroscopic data X-ray crystallographic data and molecular coordinates of computed structures (xyz). CCDC 2532060 (**7e**) contains the supplementary crystallographic data for this paper.

Acknowledgements

This work was supported by the Swiss National Science Foundation (Grants 200021_188490 and 200020_219276), the University of Geneva and the Schmidheiny Foundation. We thank Stéphane Rosset (University of Geneva) for measuring HRMS analyses, and Dr. Amalia I. Poblador-Bahamonde (University of Geneva) for offering access to her computational facilities. Parts of the computations were performed at the University of Geneva on the "Yggdrasil" and "Bamboo" HPC clusters.

Notes and references

1 (a) R. C. D. Brown and J. F. Keily, *Angew. Chem., Int. Ed*. 2001, **40**, 4496−4498. (b) *Medicinal Natural Products: A Biosynthetic Approach*, ed. P. M. Dewick, Wiley, Chichester, 2002. (c) H. Nakamura and Y. Yamamoto, *Handbook of Organopalladium Chemistry for Organic Synthesis*, Wiley-Interscience, West Lafayette, 2002, vol. 2. (d) U. Nubbemeyer, *Synthesis* 2003, **7**, 0961–1008. (e) E. Breitmaier, *Terpenes*, *Flavors*, *Fragrances*, *Pharmaca*, *Pheromones*, Wiley-VCH, Weinheim, 2006. (f) Y. Liu, X. Liu and X. Feng, *Chem. Sci.* 2022, **13**, 12290–12308.

2 (a) P. Zhang, L. A. Brozek and J. P. Morken, *J. Am. Chem. Soc.* 2010, **132**, 10686–10688. (b) P. Zhang, H. Le, R. E. Kyne and J. P. Morken, *J. Am. Chem. Soc.* 2011, **133**, 9716–9719. (c) L. A. Brozek, M. J. Ardolino and J. P. Morken, *J. Am. Chem. Soc.* 2011, **133**, 16778–16781. (d) H. Le, R. E. Kyne, L. A. Brozek and J. P. Morken, *Org. Lett.* 2013, **15**, 1432–1435. (e) M. J. Ardolino and J. P. Morken, *J. Am. Chem. Soc.* 2014, **136**, 7092–7100. (f) H. Le, A. Batten and J. P. Morken, *Org. Lett*. 2014, **16**, 2096–2099.

3 V. Hornillos, M. Pérez, M. Fañanás-Mastral and B. L. Feringa, *J. Am. Chem. Soc.* 2013, **135**, 2140–2143.

4 (a) Y. Yasuda, H. Ohmiya and M. Sawamura, *Angew. Chem., Int. Ed.* 2016, **55**, 10816–10820. (b) Y. Yasuda, H. Ohmiya and M. Sawamura, *Synthesis* 2018, **50**, 2235–2246.

5 J. Y. Hamilton, N. Hauser, D. Sarlah and E. M. Carreira, *Angew. Chem., Int. Ed.* 2014, **53**, 10759–10762.

6 H.-H. Zhang, M. Tang, J.-J. Zhao, C. Song and S. Yu, *J. Am. Chem. Soc.* 2021, **143**, 12836−12846.

7 F. Meng, K. P. McGrath and A. H. Hoveyda, *Nature* 2014, **513**, 367–374.

8 N. Vázquez-Galiñanes, G. Sciortino, M. Piñeiro-Suárez, B. L. Tóth, F. Maseras and M. Fañanás-Mastral, *J. Am. Chem. Soc.* 2024, **146**, 21977–21988.

9 C. Zhang and C. Mazet, *Org. Lett.* 2024, **26**, 5386–5390.

10 C. Zhang, B. Leforestier, C. Besnard and C. Mazet, *Chem. Sci.* 2025, **16**, 22656–22665.

11 S. Sakuragi, T. Akiba, T. Tanahashi and T. Fujihara, *Angew. Chem., Int. Ed.* 2022, **61**, e202202226.

12 G. Yamagiwa, H. Murata, K. Semba and T. Fujihara, *J. Org. Chem.* 2025, **90**, 5066–5069.

13 (a) B. M. Trost, D. L. Van Vranken and C. Bingel, *J. Am. Chem. Soc.* 1992, **114**, 9327–9343. (b) B. M. Trost, H. C. Shen, L. Dong, J.-P. Surivet and C. Sylvain, *J. Am. Chem. Soc.* 2004, **126**, 11966–11983. (c) B. M. Trost, *Tetrahedron* 2015, **71**, 5708–5733. (d) O. Pàmies, J. Margalef, S. Cañellas, J. James, E. Judge, P. J. Guiry, C. Moberg, J.-E. Bäckvall, A. Pfaltz, M. A. Pericàs and M. Diéguez, *Chem. Rev.* 2021, **121**, 4373–4505.

14 (a) S. D. Dreher, S.-E. Lim, D. L. Sandrock and G. A. Molander, *J. Org. Chem.* 2009, **74**, 3626–3631. (b) C.-T. Yang, Z.-Q. Zhang, H. Tajuddin, C.-C. Wu, J. Liang, J.-H. Liu, Y. Fu, M. Czyzewska, P. G. Steel, T. B. Marder and L. Liu, *Angew. Chem., Int. Ed.* 2012, **51**, 528–532.

15 (a) X. Cui and K. Burgess, *Chem. Rev.* 2005, **105**, 3272–3296. (b) Verendel, J. J.; Pàmies, O.; Diéguez, M.; Andersson, P. G. *Chem. Rev.* 2014, **114**, 2130–2169.

16 (a) R. H. Crabtree, *Acc. Chem. Res.* 1979, **12**, 331−337. (b) B. Wüstenberg and A. Pfaltz, *Adv. Synth. Catal.* 2008, **350**, 174−178.

17 (a) F. Weigend and R. Ahlrichs, *Phys. Chem. Chem. Phys.* 2005, **7**, 3297–3305. (b) F. Weigend, *Phys. Chem. Chem. Phys.* 2006, **8**, 1057–1065. (c) O. A. Vydrov and T. Van Voorhis, *J. Chem. Phys.* 2010, **133**, 244103. (d) W. Hujo and S. Grimme, *J. Chem. Theory Comput.* 2011, **7**, 3866–3871. (e) F. Neese, *Wiley Interdiscip. Rev. Comput. Mol. Sci.* 2012, **2**, 73–78. (f) N. Mardirossian and M. Head-Gordon *J. Chem. Phys.* 2016, **144**, 214110. (g) C. Bannwarth, S. Ehlert and S. Grimme, *J. Chem. Theory Comput.* 2019, **15**, 1652–1671. (h) S. Ehlert, M. Stahn, S. Spicher and S. Grimme, *J. Chem. Theory Comput.* 2021, **17**, 4250–4261. (i) F. Neese, *Wiley Interdiscip. Rev. Comput. Mol. Sci.* 2022, **12**, e1606. (j) F. Neese, *Wiley Interdiscip. Rev. Comput. Mol. Sci.* 2025, **15**, e70019. (k) B. M. Wood, M. Dzamba, X. Fu, M. Gao, M. Shuaibi, L. Barroso-Luque, K. Abdelmaqsoud, V. Gharakhanyan, J. R. Kitchin, D. S. Levine, K. Michel, A. Sriram, T. Cohen, A. Das, A. Rizvi, S. J. Sahoo, Z. W. Ulissi and C. L. Zitnick, *arXiv preprint* June 30, 2025 (DOI: 10.48550/arXiv.2506.23971).

18 (a) P. H. M. Budzelaar, N. N. P. Moonen, R. Gelder, J. M. M. Smits and A. W. Gal, *Eur. J. Inorg. Chem.* 2000, **4**, 753–769. (b) X. Cui, Y. Fan, M. B. Hall and K. Burgess, *Chem. Eur. J.* 2005, **11**, 6859–6868.

19 Aggregation patterns featuring multiple units of LiOAc were not investigated thus far, and a monomeric state was assumed throughout the study.

20 (a) A. V. Kalikadien and E. A. Pidko, Performance of Meta's Universal Model for Atoms across the Conformational and Configurational Space of Diverse Transition-Metal Catalysts *J. Phys. Chem. A* 2026, **130**, 1897–1904. (b) D. H. Ess, K. P. Quirion, W.-Y. Kong, B. Stanley and J. Joy, *ChemRxiv preprint*. December 18, 2025. (DOI: 10.26434/chemrxiv-2025-z1s3s). (c) J. Marks, J. Vandezande and J. Gomes, *arXiv preprint*. April 1, 2026. (DOI: 10.48550/arXiv.2604.00405).

View Article Online
DOI: 10.1039/D6SC04784J

21 F. Wu, K. Huang, Z. Cen, C. Yan, Y. Kan, X. Li and X. Wu, *ACS Catal.* 2025, **15**, 8586–8598.
22 M. Bellido, M. Garçon, X. Verdaguer and A. Riera, *Adv. Synth. Catal.* 2024, **366**, 2791–2800.
23 The nucleophilic attack proved challenging for various DFT methods, likely due to a high degree of charge transfer at the transition state, which consequently is largely over-stabilized by density functional approximations except for range-separated hybrids. See SI, section 8.2 for detail.
24 M. Méndez, J. M. Cuerva, E. Gómez-Bengoa, D. J. Cárdenas and A. M. Echavarren, *Chem. - Eur. J.* 2002, **8**, 3620–3628.
25 M. Pérez-Rodríguez, A. A. C. Braga, A. R. De Lera, F. Maseras, R. Álvarez and P. Espinet, *Organometallics* 2010, **29**, 4983–4991.
26 This corresponds to a C1/C3$_{(R)}$/C3$_{(S)}$ product distribution of 0.5/88.4/11.1, in fair agreement with the experimental results.
27 Electron-poor aryl substituents on the cyclic allylboronate salt and electron-donating substituents on the allyl acetate both led to slightly reduced enantiomeric ratios, suggesting that the electronic character of both partners influences the energy gap between the competing pro-(*R*) and pro-(*S*) reductive elimination transition states accessible from intermediates **K$_1$** and **K$_2$**.

View Article Online
DOI: 10.1039/D6SC04784J

The data supporting this article have been included as part of the SI. This includes experimental procedures, characterization of all new compounds, spectroscopic data X-ray crystallographic data and molecular coordinates of computed structures (xyz). CCDC 2532060 (**7e**) contains the supplementary crystallographic data for this paper.